Copper(II) Inhibits in Vitro Conversion of Prion Protein into Amyloid Fibrils†

Olga V. Bocharova,‡ Leonid Breydo,‡ Vadim V. Salnikov,‡ and Ilia V. Baskakov*,‡,§

Medical Biotechnology Center, University of Maryland Biotechnology Institute, Baltimore, Maryland 21201, and Department of Biochemistry and Molecular Biology, University of Maryland School of Medicine, Baltimore, Maryland 21201

Received February 10, 2005; Revised Manuscript Received March 23, 2005

ABSTRACT: In recent studies, the amyloid fibrils produced in vitro from recombinant prion protein encompassing residues 89−230 (rPrP 89−230) were shown to produce transmissible form of prion disease in transgenic mice (Legname et al., (2004) *Science 305,* 673−676). Long incubation time observed upon inoculation of the amyloid fibrils, however, suggests that the fibrils generated in vitro have low infectivity titers. These results emphasize the need to define optimal conditions for prion conversion in vitro, under which high levels of infectivity can be generated in a cell-free system. Because copper(II) has been implicated in normal and pathological functions of the prion protein, here we investigated the effect of Cu^{2+} on cell-free conversion of recombinant PrP. Our results show that at pH 7.2 and at micromolar concentrations, Cu^{2+} inhibited conversion of full-length recombinant PrP (rPrP 23−230) into amyloid fibrils. This effect was most pronounced for Cu^{2+}, and less so for Zn^{2+}, while Mn^{2+} had no effect on the conversion. Cu^{2+}-dependent inhibition of the amyloid formation was less effective at pH 6.0, at which rPrP 23−230 displays lower Cu^{2+}-binding capacity. Using rPrP 89−230, we found that Cu^{2+}-dependent inhibition occurred even in the absence of octarepeat region; however, it was less effective. Our further studies indicated that Cu^{2+} inhibited conversion by stabilizing a nonamyloidogenic PK-resistant form of α-rPrP. Remarkably, Cu^{2+} also had a profound effect on preformed amyloid fibrils. When added to the fibrils, Cu^{2+} induced long-range coiling of individual fibrils and enhanced their PK-resistance. It, however, produced only minor changes in their secondary structures. In addition, Cu^{2+} induced further aggregation of the amyloid fibrils into large clumps, presumably, through interfibrillar coordination of copper ions by octarepeats. Taken together, our studies suggest that the role of Cu^{2+} in the pathogenesis of prion diseases is complex. Because Cu^{2+} may inhibit prion replication, while at the same time stabilize disease-specific isoform against proteolytic clearance, the final outcome of copper-induced effect on progression of prion disease may not be straightforward.

A variety of neurodegenerative diseases that can be infectious, inherited, or sporadic in origin are linked to the misfolding and aggregation of the prion protein (PrP)[1] (*1*). A key event in all three forms of prion diseases is the conversion of the normal isoform of the prion protein, PrP^C, into the abnormal pathological isoform, PrP^{Sc}. This conversion involves a substantial conformational change: PrP^C is a proteinase K (PK)-sensitive α-helical monomer, whereas PrP^{Sc} is an assembled multimer characterized by enhanced resistance toward PK digestion and increased amount of β-structure (*2, 3*). The "protein only" hypothesis of prion propagation postulates that PrP^{Sc} acts as a transmissible agent and that it self-propagates its pathological conformation in an autocatalytic manner using PrP^C as a substrate (*4*).

Recombinant PrP (rPrP) was proven to be a valuable biophysical model for elucidating structural aspects of prion replication. In its α-helical conformation, rPrP resembles PrP^C, as both proteins were shown to have similar secondary and tertiary structure (*5*). The N-terminal domain of α-rPrP (residues 23−123) is highly flexible and lacks any identifiable secondary structure in the absence of Cu^{2+} (*6, 7*). In contrast, the C-terminal domain (residues 124−231) is folded and contains three α-helices and two short β-strands (*7*−*9*).

Substantial effort has been dedicated to the development of an experimental protocol for reconstitution of the infectious PrP^{Sc} from rPrP in vitro (*10*−*19*). In our previous studies using mouse rPrP encompassing residues 89−230 (Mo rPrP 89−230), we developed a cell-free conversion system that generates amyloid isoforms of rPrP 89−230 (*20, 21*). When inoculated into transgenic mice expressing only PrP 89−230, these amyloid fibrils of Mo rPrP 89−230 induced prion disease that could be efficiently transmitted to both wild-type and transgenic mice (*22*). Long incubation time observed upon inoculation of the amyloid fibrils, however, suggests that the fibrils generated in vitro have low

† This work was supported by National Institute of Health Grant NS045585 to I.V.B.

* To whom correspondence should be addressed: 725 W. Lombard St., Baltimore, MD 21201. Phone, 410-706-4562; fax, 410-706-8184. e-mail, Baskakov@umbi.umd.edu.

‡ University of Maryland Biotechnology Institute.

§ University of Maryland School of Medicine.

[1] Abbreviations: PrP, prion protein; rPrP, recombinant prion protein; rPrP 23−230, full-length recombinant PrP; rPrP 89−230, recombinant PrP encompassing residues 89−230; α-rPrP 23−230, α-helical isoform of rPrP 23−231; α-rPrP 89−230, α-helical isoform of rPrP 89−231; PrP^C, cellular isoform of the prion protein; PrP^{Sc}, disease associated isoform of the prion protein; ThT, Thioflavin T; PK, proteinase K; GdnHCl, guanidine hydrochloride; FTIR, Fourier transform infrared spectroscopy; EM, electron microscopy; EDTA, ethylenediaminetetraacetic acid; EGTA, ethyleneglycol-bis(β-aminoethyl)- tetraacetic acid; TPEN, -tetrakis-(2-pyridylmethyl)ethylenediamine.

10.1021/bi050251q CCC: $30.25
Published on Web 04/14/2005

infectivity titers. Are there any other molecules involved in production of infections prions? One may speculate that yet unidentified cellular cofactors may be required to produce fibrils with higher infectivity titers in vitro. Several classes of macromolecules and different bivalent metal ions were shown to bind to PrP and, specifically, to the N-terminal region of PrP encompassing residues 23−90 (*17, 23*−*25*). While the N-terminal region is not critical for transmission of prions (*26, 27*), this region impacts conformational diversity of PrP^{Sc} conformers (*28*) and, therefore, may also influence structural properties of fibrils generated in vitro.

Among different cofactors that bind to PrP, copper was proven to be able to modulate the pathogenesis of prion disease (*29*−*32*). Despite numerous studies, however, it still remains unclear whether copper ions promote or attenuate the prion disease (*31, 33*−*35*). The presence of copper was shown to reduce the accumulation of PrP^{Sc} in the scrapie-infected neuroblastoma cells (*31*). Furthermore, a significant delay in prion disease onset was observed when scrapie-infected animals were treated with copper (*31*). Contrary to above observations, other studies reported that copper chelation delayed the onset of prion disease (*32*). Moreover, humans with PrP genes coding for extra octarepeats, regions that bind copper ions, were found to be predisposed to familial Creutzfeldt-Jakob disease (*36*). Finally, copper was also shown to promote a conversion of rPrP 23−230 into the PK-resistant form in vitro (*34*) or to help recover the infectivity and PK-resistance of partially denatured PrP^{Sc} (*37*). Taken together, these studies illustrate the complexity of copper effects on development of prion diseases.

In an effort to understand the role of copper in formation of PrP^{Sc}, we studied the effect of copper on the cell-free conversion of full-length recombinant mouse PrP (rPrP 23−230) into amyloid fibrils. rPrP 23−230 contains several Cu^{2+}-binding sites. Up to four Cu^{2+} ions were shown to bind to the octarepeat region, which is composed of multiple tandem copies of the eight-residue sequence (*38*−*44*).The octarepeat region located between residues 60 and 91 and was found to bind Cu^{2+} in a cooperative manner (*43*) and with high selectivity (*39*−*41, 44*). An additional Cu^{2+}-binding site that binds up to two Cu^{2+} ions was identified recently within residues 92 and 111 (*45*−*47*). It is reasonable to speculate that binding of Cu^{2+} to α-rPrP may affect the pathways of misfolding and, therefore, substantially impact the physical properties of amyloid fibrils generated in vitro (*45*).

In the current studies, we investigated the effect of Cu^{2+} on cell-free conversion of recombinant mouse PrP proteins. Surprisingly, we found that Cu^{2+} inhibited conversion of rPrP 23−230 into amyloid fibrils. Cu^{2+}-dependent inhibition was less effective at pH 6.0, at which rPrP 23−230 has lower Cu^{2+}-binding capacity than at pH 7.2. Among the three metal ions tested, Cu^{2+} had the strongest effect on the conversion; Zn^{2+} had an intermediate effect, and Mn^{2+} had no effect at all. Using mouse rPrP 89−230, we showed that the octarepeat region was not required for inhibition of fibril formation; however, the presence of octarepeats resulted in a stronger effect. Our data indicated that Cu^{2+}-dependent inhibition was presumably due to formation of the nonamyloidogenic PK-resistant form of α-rPrP. Furthermore, Cu^{2+} also enhanced PK-resistance of preformed fibrils, induced long-range coiling of individual fibrils, and initiated aggregation of the amyloid fibrils into large clumps. Our studies illustrate that the potential effects of Cu^{2+} on pathogenesis of prion disease are complex and can be mediated through its interaction with both normal and disease-specific isoforms of PrP.

MATERIALS AND METHODS

Protein Expression and Purification. We thank Sylvain Lehmann for providing plasmids containing the genes encoding mouse PrP. Mouse rPrP encompassing residues 89−230, was expressed and purified as described earlier (*21*). The purified proteins were confirmed to be single species with an intact disulfide bond by SDS−PAGE and electrospray mass spectrometry.

Mouse PrP 23−231 DNA was PCR amplified from pcDNA3 plasmid containing the full-length PrP gene, inserted into pET101/D-TOPO vector (Invitrogen), and transformed into Top10 cells (Invitrogen). The transformants were tested by PCR amplification; the DNAs from the positive clones were checked by DNA sequencing and retransformed into BL21(DE3) Star cells (Invitrogen). For the expression, transformants were inoculated into 10 mL of LB/carbenicillin medium (0.1 mg/mL carbenicillin) and were grown at 37 °C for 3.5 h. The entire culture was inoculated into 90 mL of LB/carbenicillin medium and grown overnight (∼16 h). Five percent of the overnight culture was inoculated into the TB medium (300 mL) supplemented with carbenicillin (0.1 mg/mL) and grown at 37 °C until the $A_{600\ nm}$ reached 0.6. Expression was induced by addition of isopropyl-β-D-thiogalactopyranoside (Sigma) to the final concentration of 1 mM, and the culture was grown for an additional 5 h. The cells were harvested by centrifugation, resuspended in lysis buffer (50 mM Tris, 1 mM EDTA, and 100 mM NaCl, pH 8; 9 mL/g of pellet), followed by the addition of lysozyme (200 μg/mL) and PMSF (20 μg/mL) with subsequent incubation on ice for 20−40 min. Deoxycholic acid (1 mg/mL) was added followed by an incubation on ice for 20−30 min, subsequent addition of DNAse (10 μg/mL), and final incubation for 30−45 min. The lysate was centrifuged at 20 000*g* for 20 min. The resulting pellet was dissolved in IMAC buffer A (5 mL/g of pellet, 0.1 M Na_2HPO_4, 10 mM Tris, 8 M urea, and 10 mM β-mercaptoethanol, pH 8;), incubated for 2 h at room temperature, and centrifuged at 20 000*g* for 15 min to remove insoluble material. The solubilized inclusion bodies were incubated with NTA Fast Flow Sepharose resin (Amersham Biosciences, Sweden) pre-charged with Ni-ions at room temperature for 1 h in end-over-end mixer. The NTA column was washed with 5 vol of IMAC buffer A, followed by elution of rPrP in IMAC buffer B (0.1 M Na_2HPO_4, 10 mM Tris, 8 M urea, and 10 mM β-mercaptoethanol, pH 4.5). Fractions containing rPrP were diluted to a final protein concentration of 0.3 mg/mL using 9 M urea in 0.1 M Tris buffer, pH 8.0, and dialyzed against the same buffer to eliminate β-mercaptoethanol and to oxidize the protein. After oxidation, rPrP was dialyzed against the same buffer containing 10 mM EGTA. The dialyzed solution was diluted 3-fold with buffer I (0.1% trifluoroacetic acid/H_2O), loaded on a 25 mm × 25 cm C4 HPLC column (Vydac), and eluted using a gradient of buffer II (0.1% trifluoroacetic acid/acetonitrile). Fractions containing rPrP were eluted in 40% acetonitrile and lyophilized. The purified rPrP was confirmed by SDS−PAGE and electrospray mass spectrometry to be single

species with an intact disulfide bond. An amount of 20 mg of >99% pure rPrP was obtained per liter of cell culture.

In Vitro Refolding of rPrP to the α-Helical Form and to the Amyloid Fibrils. To convert rPrP 23−230 or rPrP 89−230 to the α-helical forms, stock solutions of rPrPs (130 μM) in 6 M GdnHCl were diluted to the final protein concentration of 22 μM in 10 mM Tris-HCl buffer, pH 6.5, at room temperature and dialyzed against 10 mM Tris-HCl buffer, pH 6.5.

To form amyloid fibrils, a stock solution of rPrP 23−230 (130 μM) in 6 M GdnHCl was diluted to the final protein concentration of 22 μM and incubated at 37 °C in 20 mM Na-acetate buffer (pH 5.0), 1 M GdnHCl, 3 M urea, and 150 mM NaCl with continuous shaking at 600 rpm using a Delfia plate shaker (Wallac) in conical plastic tubes (Eppendorf) in a reaction volume >0.4 mL for 36 h. The yield of fibril formation was monitored using a ThT-binding assay. Aliquots withdrawn during the time course of incubation at 37°C were diluted into 5 mM Na-acetate buffer (pH 5.5) to a final concentration of rPrP 23−230 of 0.3 μM, then ThT (Molecular Probes, Eugene, OR) was added to a final concentration of 10 μM. Six emission spectra (from 460 to 520 nm) were recorded for each sample in a 0.4 cm rectangular cuvette with excitation at 445 nm on a Fluoro-Max-3 fluorimeter (Jobin Yvon, Edison, NJ); both excitation and emission slits were 4 nm. Spectra were averaged, and the fluorescence intensity at emission maximum (482 nm) was determined. In a typical experiment, the level of ThT fluorescence increased from 50 000 CPS at time zero to 1 400 000 CPS upon 36 h of incubation as measured for 0.3 μM of rPrP 23−230. The amyloid fibrils were dialyzed against 10 mM Na-acetate buffer, pH 5.0, and stored at +4 °C.

Monitoring the Kinetics of Amyloid Formation. The effect of metal ions on the kinetics of amyloid formation was monitored using an automated format. Stock solutions of rPrP 23−230 (130 μM) or rPrP 89−230 (100 μM) in 6 M GdnHCl were diluted to the final protein concentration of 1 μM for rPrP 23−230 or 2 μM for rPrP 89−230 and incubated in 50 mM Hepes buffer (pH 7.2 or pH 6.0), 2 M GdnHCl, and 0.15 mM NaCl in the reaction volume of 0.2 mL in 96-well plates and in the presence of ThT (10 μM). Our preliminary studies using the manual format demonstrated that the presence of 10 μM ThT in the reaction mixture does not interfere with the kinetics of amyloid formation. Because ThT fluorescence was monitored directly from 96-well plates without withdrawing aliquots, we were able to reduce the concentration of rPrP 23−230 down to 1 μM in the conversion reaction. We also replaced 3 M urea used in our previous in vitro conversion protocol (*21*) with 2 M GdnHCl in the current study to minimize interactions between the buffer and divalent cations. The 96-well plates were covered by ELAS septum sheets (Spike International) and incubated at 37°C upon continuous shaking at 900 rpm in Fluoroskan Ascent CF microplate reader (ThermoLabsystems), and the kinetics was monitored by bottom-reading of fluorescence intensity every 10 min using 444 nm excitation and 485 nm emission filters. Every set of measurements was performed in triplicates, and the results were averaged. At least two sets of measurements were performed for each tested concentration of metal ions.

The kinetics of the amyloid formation monitored in an automated assay were analyzed by fitting time-dependent changes in fluorescence of ThT (F) versus time of the reaction (t) to the following equation (*48*):

$$F = A + (B + ct)/(1 + \exp[k(t_m - t)]) \quad (1)$$

where A is the initial level of ThT fluorescence during the lag-phase, B is the difference between final level of ThT fluorescence and the initial level during the lag-phase, k is the rate constant of amyloid formation (h^{-1}), t_m is the midpoint of transition, and c is the empirical parameter describing changes in ThT fluorescence after transition. The length of the lag-phase (t_l) of amyloid formation was calculated as $t_l = t_m - 2/k$.

Proteinase K Digestion. In a typical experiment, the α-helical form or the amyloid fibrils of rPrP 23−230 (0.1 mg/mL) were treated with PK at 37 °C for 1 h in 50 mM Hepes buffer (pH 7.2). Digestion was stopped by quenching with PMSF (2 mM), followed by addition of 4× sample buffer and 8 M urea to a final concentration of 3 M. Samples were heated at 95 °C for 15 min and analyzed by precast 12% NuPage SDS−PAGE (Invitrogen).

Size-Exclusion Chromatography. The aggregation of rPrP 23−230 and rPrP 89−230 was monitored by HPLC size-exclusion chromatography at 23 °C with a flow rate of 0.3 mL/min using a 4.6 mm × 30 cm TSK Super SW 3000 HPLC column (Tosoh Bioscience, Tokyo, Japan) in a running buffer of 50 mM Hepes (pH 7.0), 2 M GdnHCl, and 0.15 M NaCl. Running buffer for the samples incubated with Cu^{2+} was supplemented with 100 μM $CuCl_2$. GdnHCl was used to avoid adsorption of rPrP to the column resin.

Electron Microscopy. Negative staining was performed on carbon-coated 100-mesh grids coated with 0.01% of poly-L-lysine solution prior to staining. The samples were adsorbed for 30 s, washed with 0.1 and 0.01 M Na-acetate for 5 s each, stained with freshly filtered 2% uranyl acetate for 30 s, dried, and then viewed in a Zeiss EM 10 CA electron microscope.

FTIR and CD Spectroscopy. CD spectra of freshly prepared α-rPrP 23−230 (0.28 mg/mL) were recorded in 2 mM Hepes buffer (pH 7.2) in a 0.1-cm cuvette with a J-810 CD spectrometer (Jasco, Easton, MD), scanning at 20 nm/min, with a bandwidth of 1 nm and data spacing of 0.5 nm. Each spectrum represents the average of five individual scans after subtracting the background spectra.

FTIR spectra were measured with a Bruker Tensor 27 FTIR instrument (Bruker Optics, Billerica, MA) equipped with MCT detector cooled with liquid nitrogen. An amount of 10 μL of aqueous solution of rPrP 23−230 fibrils (0.5 mg/mL) in 50 mM Hepes buffer (pH 7.2) was loaded into BioATRcell II. A total of 256 scans at 2 cm^{-1} were collected for each sample under constant purging with nitrogen, corrected for water vapor, and background spectra of buffer were subtracted.

Real-Time Imaging by Epifluorescence Microscopy. Fibrils of rPrP 23−230 were diluted into 50 mM Hepes buffer (pH 7.2) in plastic tubes (Eppendorf) to a final concentration of rPrP 23−230 equivalent to 0.3 μM, and incubated in the absence or in the presence of 100 μM $CuCl_2$. ThT was added to a final concentration of 10 μM before measurements, a

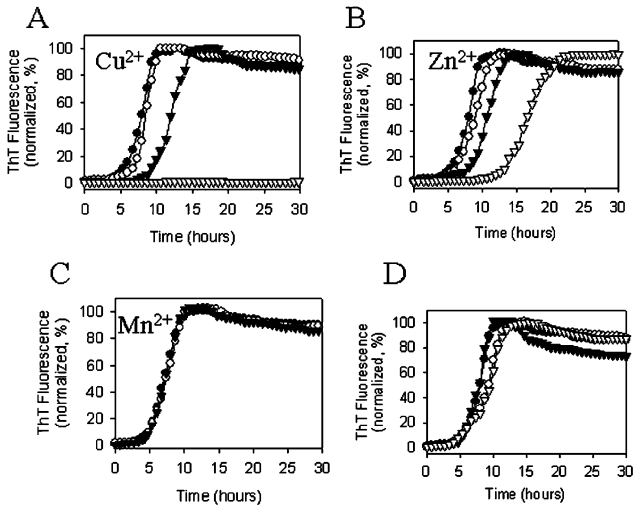

FIGURE 1: Cu^{2+} and Zn^{2+}, but not Mn^{2+}, inhibit the conversion of rPrP 23−230 into the amyloid fibrils at pH 7.2. The kinetics of fibril formation for 1 μM of rPrP 23−230 as a function of concentration of Cu^{2+} (A) at 1 μM (○), 10 μM (▼), 100 μM (▽), and in the absence of Cu^{2+} (●); as a function of concentration of Zn^{2+} (B) at 1 μM (○), 10 μM (▼), 100 μM (▽), and in the absence of Zn^{2+}(●); as a function of concentration of Mn^{2+} (C) at 100 μM (○), 1 mM (▼), and in the absence of Mn^{2+}(●); and in the presence of the following chelators (D): 10 mM EDTA (○), 1 mM EGTA (▼), and 1 mM TPEN (▽), and in the absence of chelators (●). The conversion reactions were carried out at 37 °C in 50 mM Hepes buffer (pH 7.2), 2 M GdnHCl, and 0.15 M NaCl and monitored by ThT fluorescence using the automated format.

20 μL drop was placed on a cover slip and analyzed by epifluorescence microscopy.

Epifluorescence microscopy was carried out on an inverted microscope (Nikon Eclipse TE2000-U) with illumination system X-Cite 120 (EXFO Photonics Solutions Inc.) connected through fiber-optics using a 1.3 aperture Plan Fluor 100× NA objective. The emission was isolated from Rayleigh and Raman-shifted light by a combination of filters: an excitation filter 485DF22, a beam splitter 505DRL-PO2, and an emission filter 510LP (Omega Optical, Inc.). Digital images were acquired using a cooled 12-bit CoolSnap HQ CCD camera (Photometrics).

RESULTS

Cu^{2+} and Zn^{2+}, but not Mn^{2+}, Inhibit Conversion of rPrP 23−230 into the Amyloid Fibrils at pH 7.2. The cell-free conversion of rPrP 23−230 into amyloid fibrils was monitored using automated format in 96-well plates at rPrP 23−230 concentration of 1 μM (see Materials and Methods). At pH 7.2, the conversion reaction displayed a lag-phase of 6.1 h (Figure 1A) (the length of the lag-phase was calculated as described in Materials and Methods). As judged from the length of the lag-phase, Cu^{2+} inhibited conversion of rPrP 23−230 into amyloid fibrils (Table 1). Addition of 1 μM $CuCl_2$ (1 M equiv of Cu^{2+} per rPrP 23−230) increased the lag-phase by 17%. In the presence of 10 μM of $CuCl_2$, the lag-phase increased from 6.1 to 9.8 h (by 60%). No fibrils were detected for at least 60 h of incubation in the presence of 100 μM $CuCl_2$ (Figure 1A). Thus, substantial inhibition was achieved, when more than 1 M equiv of Cu^{2+} was added to the reaction mixture.

To make sure that fibril formation was not affected by metal ions that might be copurified with rPrP 23−230, we tested the effect of three different chelating agents: EDTA, EGTA, and TPEN. If rPrP 23−230 contained substantial amount of metal ions, addition of a chelating agent would shorten the lag-phase. None of the three chelating agents was able to facilitate the conversion reaction (Figure 1D).

Table 1: Effect of Cu^{2+} and Zn^{2+} on the Length of Lag-Phase (in Hours) of rPrPs in Vitro Polymerization

			amount of $CuCl_2$ or $ZnCl_2$ in the reaction				
rPrP	ion	pH	none	1 μM	10 μM	100 μM	1 mM
rPrP 23−230	Cu^{2+}	7.2	6.1[a]	7.1	9.8	>60	−
	Cu^{2+}	6.0	8.8	8.9	13.1	18.5	−
	Zn^{2+}	7.2	6.1	6.6	8.5	13.4	−
rPrP 89−230	Cu^{2+}	7.2	20.1	21.7	33.2	52.8	−
	Zn^{2+}	7.2	20.1	−	−	32.0	43.8

[a] The length of the lag-phase are shown in hours and were calculated by fitting the kinetic curves to the eq 1 as described in Materials and Methods.

Besides Cu^{2+}, other bivalent metal ions also bind to PrP (*25*, *49*, *50*), so we tested the effect of Zn^{2+} and Mn^{2+} on the conversion reaction. We found that Zn^{2+} inhibited fibril formation; however, the efficacy of inhibition was lower than that of Cu^{2+}. In the presence of 1, 10, or 100 μM of $ZnCl_2$, the length of the lag-phase increased by 8%, 40% and 120%, respectively (Figure 1B, Table 1). Mn^{2+} did not have any notable effects on the conversion reaction even at a concentration of 1 mM (Figure 1C). These experiments demonstrated that at neutral pH, the conversion of rPrP 23−230 into amyloid conformation is efficiently inhibited by Cu^{2+} and to a less degree by Zn^{2+}, but not by Mn^{2+}. Our data are consistent with previous observation that Mn^{2+} does not bind to the octarepeat region of PrP (*44*).

Cu^{2+}-Induced Inhibition of the Amyloid Formation Is Less Effective at pH 6.0. Previous studies demonstrated that the binding stoichiometry of Cu^{2+} to the octarepeat region of PrP is pH-dependent, with four Cu^{2+} bound at pH 7.4 and only two Cu^{2+} bound at pH 6.0 (*40*−*43*). The reduced Cu^{2+}-binding capacity of PrP, as observed at pH 6.0, is believed to be due to high pH sensitivity of glycine amide−Cu linkages and/or change in protonation states of the histidine residues (*33*). Therefore, next we set to determine whether the inhibitory effect of Cu^{2+} is maintained at pH 6.0. We found that the conversion of rPrP 23−230 into fibrillar form is inhibited even at pH 6.0, however, Cu^{2+}-induced inhibition was less efficient than those observed at pH 7.2 (Figure 2, Table 1). At pH 6.0, the length of the lag-phase of amyloid formation in the absence of Cu^{2+} was longer by 44% relative to those observed at pH 7.2. This increase observed at slightly acidic pH was consistent with our previous observation of pH dependence of fibrils formation (*21*, *51*). Addition of $CuCl_2$ at 10 and 100 μM increased the lag-phase by 50% and 110%, respectively, relative to that determined at pH 6.0 in the absence of copper (Table 1). Thus, at pH 6.0, the conversion occurred even in the presence of 100 μM $CuCl_2$, whereas no fibril formation was observed at pH 7.2 in the presence of the same amount of copper for at least 60 h.

Cu^{2+} Inhibits Fibrils Formation in the Absence of Octarepeats. In addition to the octarepeat region that contains four potential Cu^{2+}-binding sites, an additional site for binding of one or two copper ions was identified within residues 92−111 (*45*−*47*). To determine whether binding of Cu^{2+} to the fifth binding site affects amyloid formation,

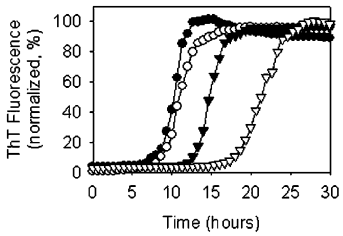

FIGURE 2: Cu^{2+} inhibits the conversion of rPrP 23−230 into the amyloid form to lesser degree at pH 6.0. The kinetics of fibril formation for 1 μM of rPrP 23−230 as a function of concentration of Cu^{2+} at 1 μM (○), 10 μM (▼), 100 μM (▽), and in the absence of Cu^{2+} (●). The conversion reactions were carried out at 37 °C in 50 mM Hepes buffer (pH 6.0), 2 M GdnHCl, and 0.15 M NaCl and monitored by ThT fluorescence using the automated format. An increase of the lag-phase observed at pH 6.0 in the absence of Cu^{2+} relative to that measured at pH 7.2 is in agreement with our previous studies of pH dependency of amyloid formation (*21*, *51*).

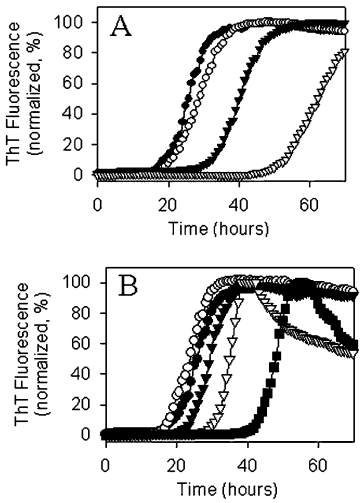

FIGURE 3: Cu^{2+} and Zn^{2+}, but not Mn^{2+}, inhibit the conversion of rPrP 89−230 into the amyloid form at pH 7.2. The kinetics of fibril formation for 2 μM of rPrP 89−230 as a function of concentration of Cu^{2+} (A) at 1 μM (○), 10 μM (▼), 100 μM (▽), and in the absence of Cu^{2+} (●); and as a function of concentration of either Mn^{2+} or Zn^{2+} (B) at 100 μM Mn^{2+}(○), 1 mM Mn^{2+}(▼), 100 μM Zn^{2+} (▽), 1 mM Zn^{2+} (■), and in the absence of metal ions (●). The conversion reactions were carried out at 37 °C in 50 mM Hepes buffer (pH 7.2), 2 M GdnHCl, and 0.15 M NaCl and monitored by ThT fluorescence using the automated format.

we used a truncated recombinant mouse PrP encompassing residues 89−230 (rPrP 89−230). In the absence of Cu^{2+}, rPrP 89−230 converts to the fibrillar form with a lag-phase of 20.1 h (Figure 3A). This result is consistent with an experimental observation in transgenic mice that elimination of the octarepeat region slows down disease progression (*52*). Addition of $CuCl_2$ at concentrations of 1, 10, and 100 μM to the reaction mixtures increased the lag-phase by 8%, 65%, and 162%, respectively (Figure 3A, Table 1). In the presence of 100 μM and 1 mM $ZnCl_2$, the length of the lag-phase increased by 59% and 118%, respectively (Figure 3B, Table 1). Mn^{2+} showed only slight inhibition at a concentration of 1 mM (Figure 3B). The copper-dependent inhibition effect is most likely mediated by the binding of Cu^{2+} to the residues 96−111. Because higher concentrations of Zn^{2+} were required to achieve the same inhibitory effect, the fifth binding site seems to have high selectivity for Cu^{2+}. Overall, these data illustrate that Cu^{2+} inhibits PrP conversion even in the absence of the octarepeat region. However, Cu^{2+}-dependent inhibition is more effective for full-length rather then for truncated rPrP.

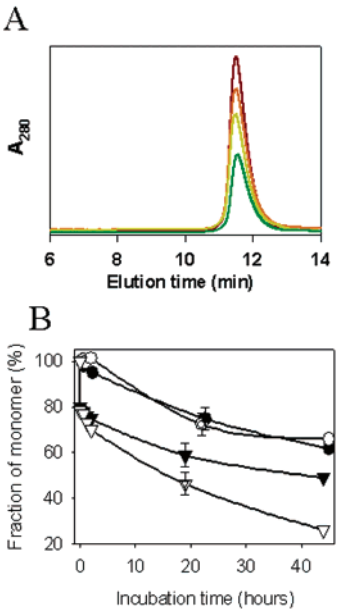

FIGURE 4: Cu^{2+} causes aggregation of α-rPrP 23−230 and α-rPrP 89−230. (A) Size-exclusion chromatography profile of original α-rPrP 23−230 (brown line) and profiles obtained upon incubation for 15 min (orange line), 2 h (yellow line), and 20 h (green line) in the presence of 100 μM Cu^{2+}. (B) The kinetics of nonspecific aggregation of the α-rPrP 23−230 (○, ▽) and the α-rPrP 89−230 (●, ▼) in the absence of copper (circles) and in the presence of 100 μM Cu^{2+} (triangles) presented as a decrease of monomer species. The α-helical forms of rPrP 23−230 (2 μM) or rPrP 89−230 (6 μM) were incubated under solvent conditions used for the conversion reaction (50 mM Hepes buffer pH 7.2, 2 M GdnHCl, and 0.15 M NaCl) at 37 °C but without shaking, and the amount of monomer form was determined by size-exclusion chromatography. Data points represent the mean ± standard deviation for triplicate samples.

Cu^{2+} Causes the Aggregation of α-rPrP 23−230 and α-rPrP 89−230. To gain insight into the mechanism of Cu^{2+}-dependent inhibition of the in vitro conversion, we set to determine whether Cu^{2+} induces nonspecific aggregation of α-rPrPs, a process which may interfere with the conversion into fibrillar form. Both α-rPrP 23−230 and α-rPrP 89−230 were incubated in the presence of 100 μM $CuCl_2$ under the same solvent conditions that were used for the conversion reaction but without shaking. In the absence of shaking, no fibrils were detected in the reaction mixture as judged from a ThT assay (data not shown). Aggregation was measured by size-exclusion chromatography based on the decrease in fraction of monomeric species (Figure 4A). In the absence of Cu^{2+}, both proteins aggregated very slowly with approximately 80% of rPrPs remaining in monomeric forms after 20 h of incubation (Figure 4B). In the presence of Cu^{2+}, the population of monomeric species of both proteins dropped down to 80% only within 15 min after the addition of $CuCl_2$ (Figure 4B). Because no species of higher oligomerization state eluted from the column even in the excluded volume (Figure 4A), Cu^{2+} seemed to have caused aggregation of rPrP into large particles, which had adsorbed to the column. rPrP 23−230 displayed a higher rate of aggregation than rPrP 89−230 did. This result is consistent with previous observations that the copper ions cause PrP aggregation and that full-length PrP is more prone to aggregation than rPrP

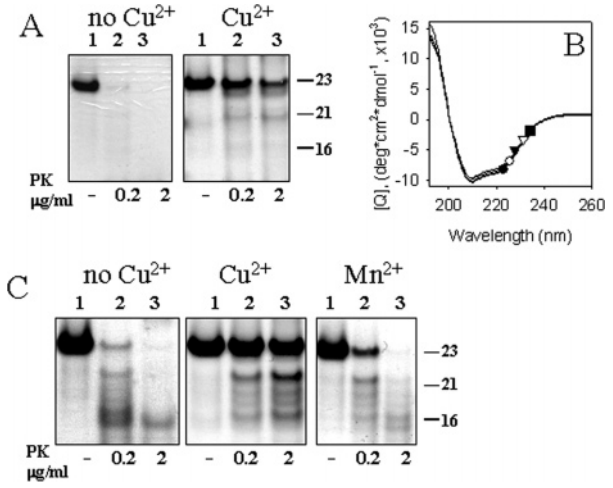

FIGURE 5: Cu^{2+} enhances PK-resistance of both isoforms, α-rPrP 23−230, and the amyloid fibrils. (A) PK-digestion of α-rPrP 23−230 preincubated in the absence (left panel) and in the presence of Cu^{2+} (right panel). (B) CD spectra of α-rPrP 23−230 (12 μM) measured in the absence of copper (λ) and with addition of 1 (○), 2 (▼), 4 (▽), and 10 (■) M equiv of Cu^{2+}. Spectra were collected in 2 mM Hepes buffer, pH 7.2. (C) PK-digestion of the amyloid fibrils preincubated with 100 μM Cu^{2+} (central panel), 100 μM Mn^{2+} (right panel), or in the absence of metal ions (left panel). The α-helical form or the amyloid fibrils of rPrP 23−230 (0.1 mg/mL, an equivalent of 8.6 μM) were incubated with 100 μM of $CuCl_2$ or $MnCl_2$ for 1 h at 37 °C in 50 mM Hepes buffer (pH 7.2) followed by digestion with PK for 1 h at 37 °C at the following PK/rPrP ratios: 1:500 by mass (lanes 2) and 1:50 (lanes 3).

89−23 (*34*, *53*, *54*). High-aggregation propensity of rPrP 23−230 may account in part for more effective Cu^{2+}-dependent inhibition of the conversion reaction for rPrP 23−230 when compared to that of rPrP 89−230.

In the presence of 100 μM Zn^{2+} or 100 μM Mn^{2+}, the levels of aggregation for both full-length and truncated α-rPrPs were the same as those observed for the same proteins without metal ions, respectively (data not shown). While 100 μM Mn^{2+} had no detectable effect on the kinetics of fibril formation and on nonspecific aggregation, 100 μM Zn^{2+} displayed a weak inhibitory effect on amyloid formation (Figure 1). Zn^{2+}-induced inhibition, however, was substantially less effective than those caused by Cu^{2+} (Table 1).

Cu^{2+} Increases PK-Resistance of Both the α-Helical and the Amyloid Forms of rPrP 23−230 at pH 7.2. Our finding that Cu^{2+} inhibits the in vitro conversion of PrP into fibrillar form seems to contradict several studies, which proposed that Cu^{2+} stimulated the conversion of PrP^C into PrP^{Sc} (*32*, *34*, *37*). In these studies, Cu^{2+} was shown to promote a conversion of rPrP 23−230 into the PK-resistant form (*34*) or to help recover the infectivity and PK-resistance of partially denatured PrP^{Sc} (*37*). Therefore, next we were interested to determine whether Cu^{2+} stimulates the conversion of α-rPrP 23−230 into PK-resistant conformation.

We found that in the absence of copper, α-rPrP 23−230 was fully digested upon treatment with low concentration of PK (0.2 μg/mL of PK, PK/rPrP ratio 1:500) (Figure 5A, left panel). Upon incubation with 100 μM of $CuCl_2$ for 1 h, a substantial fraction of full-length rPrP polypeptides remained intact even after treatment with 10-fold higher concentration of PK (PK/rPrP ratio 1:50) (Figure 5A, right panel). Previous studies showed that PK activity is not affected by the addition of 100 μM $CuCl_2$ (*34*, *55*); therefore, an increase of PK-resistance must be attributed to the direct effect of copper ions on proteolytic stability of α-rPrP 23−230. The PK-resistant form generated in the presence of Cu^{2+} is clearly different from PrP^{Sc} or PrP-res, since it is not digested to the PrP 27−30-like fragment and remains as a full-length rPrP.

To test whether an increase in PK-resistance of α-rPrP 23−230 upon adding Cu^{2+} is accompanied by a change in secondary structure, we employed circular dichroism spectroscopy. As judged from CD spectroscopy, addition of 1, 2, 4, or 10 M equiv of Cu^{2+} did not change the predominantly α-helical conformation of α-rPrP 23−230 (Figure 5B). Lack of conformational change was in good agreement with a previous observation that Cu^{2+} does not affect conformation of α-rPrP 23−230, if the protein is freshly prepared (*34*). Taken together, these data demonstrate that binding of Cu^{2+} inhibits amyloid formation by converting α-rPrP 23−230 into the PK-resistant nonamyloidogenic form, while it does not change the helical conformation of α-rPrP 23−230. Our data are consistent with the observations that copper converts PrP^C into the PK-resistant species that is distinct from PrP^{Sc} (*35*, *56*).

Because Cu^{2+} was also shown to enhance PK-resistance of PrP^{Sc} (*55*), we were interested to test the effect of $CuCl_2$ on preformed amyloid fibrils. First, we found that fibrils not exposed to Cu^{2+} were more resistant to treatment with PK, as compared to Cu^{2+}-free α-rPrP 23−230. These fibrils produced a minor 16-kDa band upon digestion at the PK/rPrP ratio of 1:50 (Figure 5C, left panel). In our previous studies using epitope mapping, we demonstrated that the 16-kDa proteolytic product is formed as a result of the cleavage of the N-terminal region up to the residue ∼90, leaving the C-terminal domain intact (*51*). Therefore, in the absence of Cu^{2+}, the N-terminal domain maintains the PK-sensitive conformation in fibrillar form. Upon incubation with 100 μM $CuCl_2$ followed by PK treatment at PK/rPrP ratio 1:50, the amyloid fibrils retained a substantial fraction of full-length polypeptide (23 kDa band) and displayed several partially resistant fragments with molecular weights in the range of 16 to 21 kDa (Figure 5C, central panel). Therefore, binding of Cu^{2+} enhances PK-resistance of the amyloid fibrils, presumably through stabilization of the N-terminal octarepeat region. Addition of 100 μM $MnCl_2$ instead of $CuCl_2$, induces a very minor stabilizing effect, if any (Figure 5C, right panel). Taken together, our results demonstrate that binding of Cu^{2+} stabilizes the PK-resistant conformation of the N-terminal region in both α-rPrP 23−230 and fibrillar forms.

Cu^{2+} Induces Long-Range Coiling in the Amyloid Fibrils and Produces Minor Changes in Their Secondary Structures. Substantial effort has been devoted to study the effect of Cu^{2+} on the conformation and biological properties of PrP^C, whereas the interaction of Cu^{2+} and PrP^{Sc} has not yet been explored in detail. In recent studies, Collinge and co-workers demonstrated that differences in metal ion occupancy may affect the length of the PK-resistant core of PrP^{Sc} (*57*). The same result, however, could be also attributed to substantial change in PK-activity observed at slightly different pH values (*58*).

To test whether Cu^{2+} affects secondary or higher order structure of amyloid fibrils, we employed electron microscopy (EM) and Fourier transform infrared spectroscopy

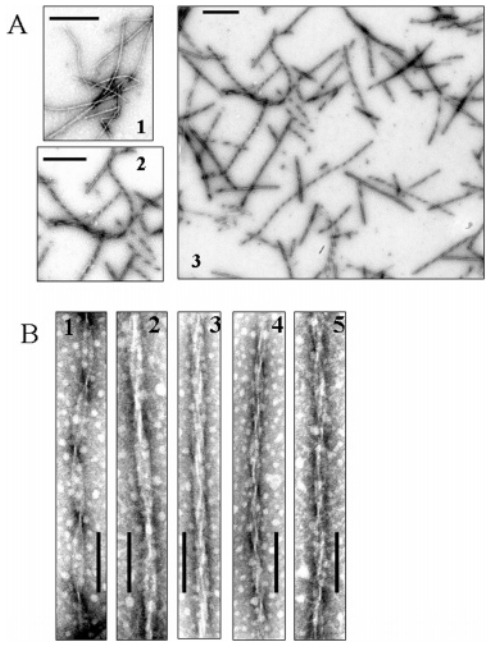

FIGURE 6: Cu^{2+} induces helical twists in amyloid fibrils as judged by electron microscopy. (A) Electron micrographs of negatively stained amyloid fibrils before (panel 1) and after incubation with 100 μM of $CuCl_2$ (panels 2 and 3). Scale bars = 1 μm. (B) Gallery of fibrils treated with Cu^{2+}. Scale bars = 0.3 μm.

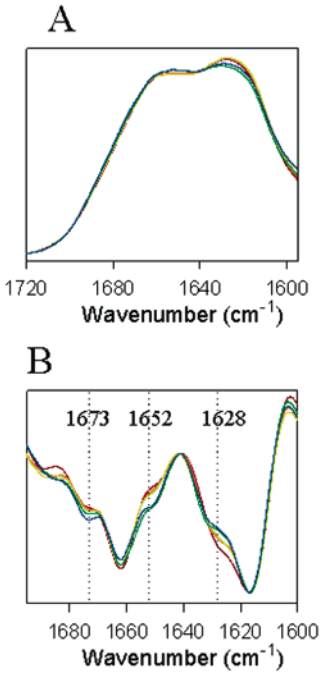

FIGURE 7: Cu^{2+} causes minor change in secondary structure of the amyloid fibrils. FTIR spectra (A) and their second derivatives (B) of the amyloid fibrils of rPrP 23−230 (20 μM) recorded in the absence of Cu^{2+} (red lines) and with addition of 1 (orange lines), 2 (yellow lines), 5 (green lines), and 15 (blue lines) M equiv of Cu^{2+}.

(FTIR). Using EM, we observed nontwisted or occasionally twisted ribbon-like structures in samples with amyloid fibrils that were not exposed to Cu^{2+} (Figure 6A, panel 1). Fibrils treated with 100 μM $CuCl_2$ showed repeating variation in width, indicative of a helical arrangement of protofilaments into long-range coiling structures (Figure 6A, panels 2 and 3). Twisted fibrils displayed diverse morphologies characterized by different width and pitch (Figure 6B). All of the morphologies with distinct long-range coiling were found in the same preparations; however, the type of fibril shown in panel 1 (Figure 6B) was the most abundant. Each fibril maintained its individual type of long-range coiling throughout the whole fibrillar structure.

Similar coiling morphologies were described for amyloid fibrils formed by other proteins such as insulin and SH3 (*59*, *60*) and peptidomimetic polymers (*61*). By studying amyloid fibrils of insulin, Saibil and co-workers proposed that the long-range twist may arise from a small interstrand angle between successive β-strands that constitute an individual fibril (*60*). In accordance with this model, even small changes in the interstrand angle will have a dramatic impact on the long-range twist, which may produce fibrils with different morphologies. Each type of long-range coiling is propagated throughout individual fibrils generating assemblies peculiar to each particular fibril. Noteworthy, high-resolution atomic force microscopy studies indicated that ribbon-like fibrils are capable of a cooperative transformation into twisted, highly ordered superhelices (*62*). One may speculate that binding of Cu^{2+} to the N-terminal region of assembled PrP polypeptides may influence the interstrand angle between successive β-strands, therefore, determining distinct type of long-range coiling in individual fibrils. Considering that there are several alternative ways by which Cu^{2+} can be coordinated by the octarepeats, this model provides a plausible explanation for the Cu^{2+}-induced changes of fibrillar morphology.

To test the extent to which binding of Cu^{2+} influences the secondary structure of amyloid fibrils, we employed FTIR spectroscopy. FTIR measurements were carried out using a BioATR (attenuated total reflectance) cell, which allows spectra to be collected from aqueous solution. In the absence of Cu^{2+}, the FTIR spectra of amyloid fibrils showed a major band at 1618 cm^{-1}, characteristic of β-sheet structures with strong intermolecular hydrogen bonds, and a smaller band at 1662 cm^{-1} that can be largely assigned to loop components (1660−1666 cm^{-1} region) with plausible contribution of turns (1670−1680 cm^{-1} region) and α-helices (1650−1660 cm^{-1} region) (Figure 7). Cu^{2+} induced only minor changes in the secondary structure of fibrils. Upon titration of fibrils with $CuCl_2$, we observed a slight increase in the absorbance intensity of shoulders near 1673 and 1652 cm^{-1}, which indicates an increase in the amount of turns and α-helical structures, respectively. The relative intensity of bands centered at 1618 and 1662 cm^{-1} remained stable (Figure 7B). In parallel, we observed a gradual decrease of a shoulder near 1628 cm^{-1}. Although the assignment of this band is not straightforward, bands centered between 1628 and 1640 cm^{-1} are commonly observed for β-sheets in many classes of globular proteins and assigned to β-sheet structures with high dynamic flexibility (*63*). Taken together, the FTIR spectroscopic analysis revealed only minor changes in secondary structure and confirmed that β-sheet structures with strong intermolecular hydrogen bonds remained stable.

Cu^{2+} Induces Aggregation of Amyloid Fibrils into Large Clumps. While studying the effect of Cu^{2+} on preformed fibrils, we noticed that, in the presence of Cu^{2+}, the fibrils have a much higher tendency for aggregation. Aggregation of the fibrils can be observed in "real time" using epifluorescent microscopy. In contrast to other imaging techniques, fluorescent microscopy enables observation of

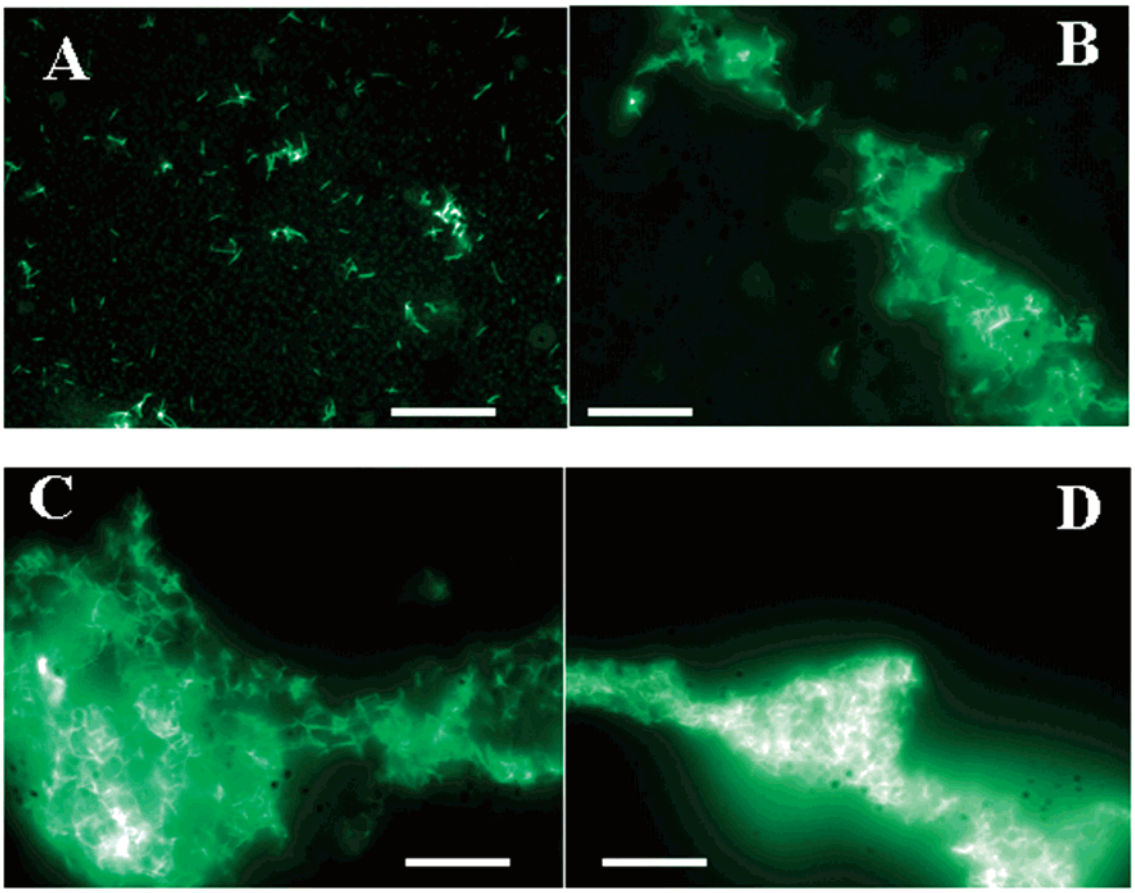

FIGURE 8: Epifluorescent microscopy of Cu^{2+}-induced aggregation of the amyloid fibrils in solution. Fluorescent images of amyloid fibrils in 50 mM Hepes buffer, pH 7.2, incubated for 1 h in the absence of Cu^{2+} (A), and incubated in the presence of 100 μM $CuCl_2$ for 5 min (B), 20 min (C), and 1 h (D) at room temperature. Amyloid fibrils were prepared as described in Materials and Methods and diluted with Hepes buffer (pH 7.2) to the final concentration of rPrP 23−230 equivalent to 0.3 μM. Scale bars = 5 μm.

macromolecular structures under near-native conditions. In the absence of Cu^{2+}, the fibrils aggregated very slowly and formed only small clusters (Figure 8A). Addition of $CuCl_2$ at pH 7.2 induced much faster coaggregation of the fibrils, and triggered formation of larger clumps (Figure 8B). The density of the amyloid clumps increased upon further incubation with $CuCl_2$ (Figure 8C,D).

DISCUSSION

Cu^{2+} is believed to play an important role in the pathogenesis of prion diseases. Recent studies have demonstrated that scrapie infection modulates copper content on a cellular level (*64*). Elimination of copper binding octarepeats slowed the rate of progression of prion disease in transgenic mice (*52*), whereas insertion of extra octarepeats made humans predisposed to Creutzfeldt-Jakob disease (*36*). While implication of copper in prion maladies has been well-established, it still remains unclear whether Cu^{2+} facilitates or attenuates prion diseases. In particular, copper was shown to delay the age at onset of prion disease and reduce the accumulation of PrP^{Sc} in the scrapie-infected neuroblastoma cells (*31*). On the other hand, another study reported that removal of copper by chelation is capable of delaying the onset of prion disease (*32*). Furthermore, consistent with the suggestion that Cu^{2+} stimulates prion conversion, copper has been shown to help recover the infectivity and PK-resistance of partially denatured PrP^{Sc} (*37*).

In the current studies, we demonstrated that Cu^{2+} inhibits in vitro conversion of the full-length and truncated mammalian prion proteins into amyloid fibrils (Figure 9). Inasmuch as polymerization of recombinant PrPs into fibrillar form captures important features of the prion replication in vivo, our studies can provide new important insight into the role of Cu^{2+} in prion diseases. In an assay conducted at neutral pH and physiological concentrations of rPrP 23−230, we showed that efficient inhibition could be observed at concentrations of Cu^{2+} between 10 and 100 μM. These concentrations are slightly above the dissociation constants measured for Cu^{2+} binding to the octarepeats, which were determined to be in the low-micromolar range (*29*, *40*, *41*, *43*). When the average extracellular Cu^{2+} concentration in the CNS greater than 10 μM and the possible local Cu^{2+} concentration in excess of 100 μM as a result of neuronal depolarization (*65*) are considered, our studies suggest that Cu^{2+} may play a key role in modulating the rate of prion propagation in vivo.

Inhibition of rPrP polymerization by metal ions was shown to be selective for Cu^{2+}, with Zn^{2+} being less effective, while Mn^{2+} was not effective at all (Figure 1). Binding of metal ions to the octarepeats displayed similar rank of selectivity, where Cu^{2+} was found to have the highest, and Mn^{2+} the lowest, affinity among the three metal ions (*35*, *40*, *41*, *50*). Furthermore, previous studies have demonstrated that the binding stoichiometry of Cu^{2+} to the octarepeat region of

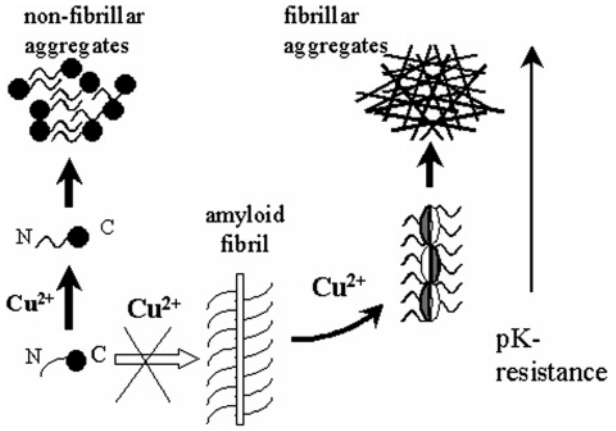

FIGURE 9: Schematic diagram illustrating complex effect of Cu^{2+} on the cell-free conversion of prion protein. Cu^{2+} inhibits conversion of α-rPrP 23−230 into amyloid fibrils by stabilizing nonamyloidogenic PK-resistant form of α-rPrP 23−230. PK-resistant α-rPrP 23−230 slowly forms nonfibrillar aggregates. Treatment of preformed amyloid fibrils with Cu^{2+} induces long-range coiling. When fibrils are exposed to Cu^{2+} in solution, they show high tendency for aggregation and form large clumps. Cu^{2+}-induced enhancement of PK-resistance is shown by an arrow.

PrP is highly pH-dependent, with up to four Cu^{2+} bound at pH 7.4 and only two Cu^{2+} bound at pH 6.0 (*40*−*43*). Our finding that the inhibitory effect of Cu^{2+} is attenuated at pH 6.0 is consistent with a decrease in Cu^{2+}-binding capacity of octarepeats observed at acidic pH (Figure 2). Because the conversion of PrP^C into PrP^{Sc} may occur in endosomes or lysosomes with their slightly acidic pH, our results on pH-dependence of Cu^{2+}-induced inhibition has important implication for prion replication in a cell. If prion conversion occurs in extracellular milleu with its neutral pH, one may speculate that this process should be suppressed to large extent in the presence of 100 μM Cu^{2+}. On the other hand, if the conversion of PrP occurs in lysosomes at pH 6.0 or below, the same concentration of Cu^{2+} would not be as effective.

Using a different experimental model of PrP conversion that utilizes low-percentage of SDS, Giese and coauthors showed that Mn^{2+} enhances aggregation of full-length rPrP in vitro, whereas Cu^{2+} inhibits PrP aggregation and blocks the effect of manganese (*66*, *67*). Consistent with our finding, the inhibitory effect of Cu^{2+} was assigned to the binding of Cu^{2+} to the octarepeats region of monomeric PrP (*67*). However, the Mn^{2+}-induced aggregation was shown to be mainly due to the association of preformed PrP oligomers into larger nonfibrillar aggregates. Because formation of the PrP oligomers seems to be specific for the SDS conversion assay, this may account for the differences in effects of Mn^{2+} observed in two conversion assays. Mn^{2+}-induced aggregation was also shown to be mediated through yet unknown binding sites, which are different from the octarepeats (*67*).

The current studies showed that Cu^{2+} enhances PK-resistance of α-rPrP 23−230. This finding strongly supports previous observation by Harris and co-workers, who demonstrated that copper converts PrP^C into a protease-resistant species that is distinct from scrapie isoform (*35*, *56*). Therefore, when PK-digestion assay only is used, it is easy to confuse conversion of PrP into disease-specific conformation with enhancement of PK-resistance of α-rPrP or PrP^C. On the other hand, we found that Cu^{2+} also stabilizes the fibrillar form of rPrP 23−230 against PK-digestion, an observation that supports the finding that Cu^{2+} helps to recover PK-resistance and infectivity of partially denatured PrP^{Sc} (*37*). Taken together, our data are consistent with a model, in which Cu^{2+}-induced changes in physical properties of α-rPrP (or PrP^C) are not related to the pathway of PrP^{Sc} formation (Figure 9). Specifically, this model proposes that Cu^{2+} inhibits the conversion of α-rPrP into disease-specific isoform by stabilizing a nonamyloidogenic PK-resistant form of α-rPrP. At the same time, Cu^{2+} also enhances PK-resistance of the fibrillar form. The model explains the data reported in earlier published studies, which otherwise seem contradictory.

In addition to the binding of Cu^{2+} to the N-terminal part of PrP, several Cu^{2+}-binding sites were found in the C-terminal domain (within residues 121−231) (*68*, *69*). The C-terminal binding sites showed three different Cu^{2+} coordination types and, in contrast to the octarepeats region, bound Cu^{2+} at acidic pH between 3 and 5 (*68*). Binding of Cu^{2+} to the C-terminal region opens the possibility for an additional mechanism of modulation of prion replication. Because the interaction of Cu^{2+} with the C-terminal domain is affected in some variants of PrP that are linked to the inherited forms of prion disease, a disbalance in metal ions may also have implication for familial human diseases (*69*). However, this topic needs to be addressed in future studies.

In the current studies, we demonstrated that Cu^{2+} inhibited the conversion of rPrP 89−230 into amyloid fibrils at neutral pH; however, its effect was less profound than those observed for rPrP 23−230. Inhibition of rPrP 89−230 polymerization showed selectivity for Cu^{2+}, while Zn^{2+} and Mn^{2+} were substantially less effective. In a way similar to rPrP 23−230, titration of rPrP 89−230 with Cu^{2+} did not change α-helical conformation of protein (data not shown). Our data contravenes a recent report, in which Cu^{2+} was shown to induce β-sheet formation in the PrP-derived peptide spanning residues 91−115 (*45*). It remains to be determined whether different results observed in two studies can be attributed to the differences in the length and concentrations of model polypeptides (1−12 μM of rPrP 89−230 and rPrP 23−230 used in this study versus 0.08−0.6 mM of PrP 91−115 used by Jones et al. in ref *45*) and/or to the differences in PrP sequences within the region 91−115 (mouse PrP in this study versus human PrP in ref *45*). Noteworthy, in addition to His96 and His111, sulfur of Met109 is believed to participate in coordination of Cu^{2+} by human rPrP 90−231 (*70*). Because Met109 is replaced by Leu in mouse PrP, a complex of Cu^{2+} with mouse rPrP 89−230 may have different physical properties relative to that displayed by a complex of Cu^{2+} with human rPrP 89−230.

We found that binding of Cu^{2+} to preformed amyloid fibril changed fibrillar architecture and the state of assembly. Specifically, (i) Cu^{2+} induced long-range coiling of individual fibrils (Figure 6) and (ii) stimulated fibril aggregation (Figure 8). FTIR analyses revealed only minor changes in secondary structure of fibrils upon addition of Cu^{2+}, confirming that fibrils maintained their rigid β-sheet structure. At the same time, binding of Cu^{2+} induced long-range coiling. Different types of coiling were found in the same preparation. It is reasonable to speculate that the differences in fibrillar coiling can be attributed to distinct Cu^{2+}-binding modes. Several

active binding modes are possible for coordination of Cu^{2+} by the octarepeats of α-rPrP 23−230 depending on copper occupancy and solvent conditions (*42*, *43*, *46*, *71*). Moreover, different types of Cu^{2+} site geometries were described depending on whether coordination occurs via inter-repeat or intra-repeat binding modes, where inter-repeat binding can be both intramolecular and intermolecular (*72*). Whether Cu^{2+}-binding modes in the amyloid fibrils are the same as those found in α-rPrP remains to be determined. Considering high local concentration of octarepeats in assembled fibrils, intermolecular Cu^{2+} coordination is quite plausible. Notably, each particular type of long-range coiling can be propagated throughout the length of individual fibrils. The idea that distinct types of long-range coiling may provide structural basis for the multiple strains of self-propagating aggregates has been discussed in the literature (*60*). It would be interesting to determine whether a particular type of long-range coiling can be produced as the predominant type under specific solvent conditions and whether fibrils with the particular long-range coiling could nucleate further polymerization of fibrils producing the same morphology.

Remarkably, in addition to long-range coiling, we observed that Cu^{2+} induced aggregation of amyloid fibrils into large clumps of irregular shapes (Figure 8). It is quite likely that intermolecular and interfibrillar coordination of Cu^{2+} by the octarepeat region served as a driving force for this type of aggregation. Observation of further aggregation of rPrP 23−230 fibrils into large clumps is important in light of the fact that progression of prion disease is accompanied by accumulation of amyloid prion plaques rather than of separately laying fibrils. Prion plaques vary dramatically with respect to their sizes and shapes and include kuru-type "spiked ball" plaques, "florid plaques" observed in new variant Creutzfeldt Jakob disease, small punctate deposits found in kuru as well as in some CJD cases, and other deposits (*73*). Importantly, electron microscopy studies revealed that the amyloid prion plaques have a filamentous ultrastructure similar to amyloid fibrils (*74*). Considering that amyloid fibrils generated in vitro are prone to further aggregation and that the shape and size of these aggregates are very sensitive to experimental conditions, it is understandable why the morphology of PrP^{Sc} deposits formed in the brain under pathological conditions can also be highly variable. Microenvironment and microglia may play an important role in the formation of plaques of different shape in the transmissible spongiform encephalopathies.

This work significantly extends previous biophysical studies on the interaction of copper and PrP, most of which have exploited synthetic peptides or recombinant PrP folded into α-helical conformation. Taken together, our studies suggest that the role of copper in the pathogenesis of prion diseases is complex. Depending on circumstances, Cu^{2+} may have opposing effects on development of prion diseases. From one perspective, Cu^{2+} inhibits the conversion of the prion protein into disease-specific conformation. On the other hand, Cu^{2+} can stabilize PrP^{Sc} by converting it into a more proteolytically resistant form, a process that eventually reduces the rate of PrP^{Sc} clearance. Because development of prion disease is controlled by a fine dynamic balance between the rates of PrP^{Sc} formation versus its clearance (*75*, *76*), the final outcome of copper-induced effect on progression of prion disease may not be straightforward.

REFERENCES

1. Prusiner, S. B. (1997) Prion diseases and the BSE crisis, *Science 278*, 245−251.
2. Pan, K.-M., Baldwin, M., Nguyen, J., Gasset, M., Serban, A., Groth, D., Mehlhorn, I., Huang, Z., Fletterick, R. J., Cohen, F. E., and Prusiner, S. B. (1993) Conversion of α-helices into β-sheets features in the formation of the scrapie prion proteins, *Proc. Natl. Acad. Sci. U.S.A. 90*, 10962−10966.
3. Caughey, B. W., Dong, A., Bhat, K. S., Ernst, D., Hayes, S. F., and Caughey, W. S. (1991) Secondary structure analysis of the scrapie-associated protein PrP 27−30 in water by infrared spectroscopy, *Biochemistry 30*, 7672−7680.
4. Prusiner, S. B. (1982) Novel proteinaceous infectious particles cause scrapie, *Science 216*, 136−144.
5. Hornemann, S., Schorn, C., and Wuthrich, K. (2004) NMR structure of bovine prion protein isolated from healthy calf brain, *EMBO Rep., 5*, 1159−1164.
6. Riek, R., Hornemann, S., Wider, G., Glockshuber, R., and Wüthrich, K. (1997) NMR characterization of the full-length recombinant murine prion protein, *m*PrP(23−231,. *FEBS Lett*, *413*, 282−288.
7. Donne, D. G., Viles, J. H., Groth, D., Mehlhorn, I., James, T. L., Cohen, F. E., Prusiner, S. B., Wright, P. E., and Dyson, H. J. (1997) Structure of the recombinant full-length hamster prion protein PrP(29−231): the N terminus is highly flexible, *Proc. Natl. Acad. Sci. U.S.A. 94*, 13452−13457.
8. Riek, R., Hornemann, S., Wider, G., Billeter, M., Glockshuber, R., and Wüthrich, K. (1996) NMR structure of the mouse prion protein domain PrP(121−231), *Nature 382*, 180−182.
9. James, T. L., Liu, H., Ulyanov, N. B., Farr-Jones, S., Zhang, H., Donne, D. G., Kaneko, K., Groth, D., Mehlhorn, I., Prusiner, S. B., and Cohen, F. E. (1997) Solution structure of a 142-residue recombinant prion protein corresponding to the infectious fragment of the scrapie isoform, *Proc. Natl. Acad. Sci. U.S.A. 94*, 10086−10091.
10. Jackson, G. S., Hosszu, L. L. P., Power, A., Hill, A. F., Kenney, J., Saibil, H., Craven, C. J., Waltho, J. P., Clarke, A. R., and Collinge, J. (1999) Reversible conversion of monomeric human prion protein between native and fibrilogenic conformations, *Science, 283*, 1935−1937.
11. Baskakov, I. V., Legname, G., Prusiner, S. B., and Cohen, F. E. (2001) Folding of prion protein to its native α-helical conformation is under kinetic control, *J. Biol. Chem., 276*, 19687−19690.
12. Rezaei, H., Choiset, Y., Eghiaian, F., Treguer, E., Mentre, P., Debey, P., Grosclaude, J., and Haertle, T. (2002) Amyloidogenic unfolding intermediates differentiate sheep prion protein variants, *J. Mol. Biol., 322*, 799−814.
13. Lee, S., and Eisenberg, D. (2003) Seeded conversion of recombinant prion protein to a disulfide-bonded oligomer by a reduction−oxidation process, *Nat. Struct. Biol., 10*, 725−730.
14. Kazlauskaite, J., Sanghera, N., Sylvester, I., Venien-Bryan, C., and Pinheiro, T. J. (2003) Structural changesof the prion protein in lipid membranes leading to aggregation and fibrillization, *Biochemistry, 42*, 3295−3304.
15. Sokolowski, F., Modler, A. J., Masuch, R., Zirwer, D., Baier, M., Lutsch, G., M. D. A., Gast, K., and Naumann, D. (2003) Formation of critical oligomers is a key event during conformational transition of recombinant syrian hamster prion protein, *J. Biol. Chem. 278*, 40481−40492.
16. Torrent, J., Alvarez-Martinez, M. T., Heitz, F., Liautard, J. P., Balny, C., and Lange, R. (2003) Alternative prion structural changes revealed by high pressure, *Biochemistry 42*, 1318−1325.
17. Cordeiro, Y., Machado, F., Juliano, L., Juliano, M. A., Brentani, R. R., Foguel, D., and Silva, J. L. (2001) DNA converts cellular prion protein into the beta-sheet conformation and inhibits prion peptide aggregation, *J. Biol. Chem. 276*, 49400−49409.
18. Swietnicki, W., Morillas, M., Chen, S. G., Gambetti, P., and Surewicz, W. K. (2000) Aggregation and fibrillization of the recombinant human prion protein huPrP90−231, *Biochemistry 39*, 424−431.
19. Baskakov, I. V., Legname, G., Gryczynski, Z., and Prusiner, S. B. (2004) The peculiar nature of unfolding of human prion protein, *Protein Sci. 13*, 586−595.
20. Baskakov, I.V., Legname, G., Baldwin, M. A., Prusiner, S. B., and Cohen, F. E. (2002) Pathway complexity of prion protein assembly into amyloid, *J. Biol. Chem. 277*, 21140−21148.

21. Baskakov, I. V. (2004) Autocatalytic conversion of recombinant prion proteins displays a species barrier, *J. Biol. Chem. 279*, 586−595.
22. Legname, G., Baskakov, I. V., Nguyen, H.-O. B., Riesner, D., Cohen, F.E., DeArmond, S. J., and Prusiner, S. B. (2004) Synthetic mammalian prions, *Science 305*, 673−676.
23. Gabus, C., Derrington, E., Leblanc, P., Chnaiderman, J., Dormont, D., Swietnicki, W., Morillas, M., Surewicz, W. K., Marc, D., Nandi, P., and Darlix, J. L. (2004) The prion protein has RNA binding chaperoning properties characteristic of nucleocasid protein NCP7 of HIV-1, *J. Biol. Chem. 276*, 19301−19309.
24. Warner, R. G., Hundt, C., Weiss, S., and Turnbull, J. E. (2002) Identification of the heparan sulfate binding sites in the cellular prion protein, *J. Biol. Chem. 277*, 18421−18430.
25. Gonzalez-Iglesias, R., Pajares, M. A., Espinosa, C. O. J. C., Oesch, B., and Gasset, M. (2002) Prion protein interaction with glycosaminoglycan occurs with the formation of oligomeric complexes stabilized by Cu(II) bridges, *J. Mol. Biol. 319*, 527−540.
26. Prusiner, S. B., McKinley, M. P., Bowman, K. A., Bolton, D. C., Bendheim, P. E., Groth, D. F., and Glenner, G. G. (1983) Scrapie prions aggregate to form amyloid-like birefringent rods, *Cell 35*, 349−358.
27. Fischer, M., Rülicke, T., Raeber, A., Sailer, A., Moser, M., Oesch, B., Brandner, S., Aguzzi, A., and Weissmann, C. (1996) Prion protein (PrP) with amino-proximal deletions restoring susceptibility of PrP knockout mice to scrapie, *EMBO J. 15*, 1255−1264.
28. Lawson, V. A., Priola, S. A., Meade-White, K., Lawton, M., and Chesebro, B. (2004) Flexible N-terminal region of prion protein influences conformation of protease resistant prion protein isoforms associated with cross-species scrapie infection in vivo and in vitro, *J. Biol. Chem. 279*, 13689−13695.
29. Brown, D. R., Qin, K., Herms, J. W., Madlung, A., Manson, J., Strome, R., Fraser, P. E., Kruck, T., von Bohlen, A., Schulz-Schaeffer, W., Giese, A., Westaway, D., and Kretzschmar, H. (1997) The cellular prion protein binds copper in vivo, *Nature 390*, 684−687.
30. Pattison, I. H., and Jebbett, J. N. (1971) Histopathological similarities between scrapie and cuprizone toxocity in mice, *Nature 230*, 115−117.
31. Hijazi, N., Shaked, Y., Rosenmann, H., Ben-Hur, T., and Gabizon, R. (2003) Copper binding to PrPC may inhibit prion disease propagation, *Brain Res.* 993, 192−200.
32. Sigurdsson, E. M., Brown, D. R., Alim, M. A., Scholtzove, H., Carp, R., Meeker, H. C., Prelli, F., Frangione, B., and Wisniewski, T. (2003) Copper chelation delayes the onset of prion disease, *J. Biol. Chem. 278*, 46199−46202.
33. Millhauser, G. L. (2004) Copper binding in the prion protein, *Acc. Chem. Res. 37*, 79−85.
34. Qin, K., Yang, D. S., Yang, Y., Chishti, M. A., Meng, L. J., Kretzchmar, H. A., Yip, C. M., Fraser, P. E., and Westaway, D. (2000) Copper(II)-induced conformational changes and proteasae resistance in recombinant and cellular PrP, *J. Biol. Chem. 275*, 19131.
35. Quaglio, E., Chiesa, B., and Harris, D. (2001) Copper converts the cellular prion protein into a protease-resistant species that is distinct from the scrapie isoform, *J. Biol. Chem. 276*, 11432−11438.
36. Goldfarb, L. G., Brown, P., McCombie, W. R., Goldgaber, D., Swergold, G. D., Wills, P. R., Cervenakova, L., Baron, H., Gibbs, C. J., Jr., and Gajdusek, D. C. (1991) Transmissible familial Creutzfeldt-Jakob disease associated with five, seven, and eight extra octapeptide coding repeats in the *PRNP* gene, *Proc. Natl. Acad. Sci. U.S.A. 88*, 10926−10930.
37. McKenzie, D., Bartz, J., Mirwald, J., Olander, D., Marsh, R., and Aiken, J. (1998) Reversibility of scrapie inactivation is enhanced by copper, *J. Biol. Chem. 273*, 25545−25547.
38. Hornshaw, M. P., McDermott, J. R., Candy, J. M., and Lakey, J. H. (1995) Copper binding to the N-terminal tandem repeat region of mammalian and avian prion protein: structural studies using synthetic peptides, *Biochem. Biophys. Res. Commun. 214*, 993−999.
39. Hornshaw, M. P., McDermott, J. R., and Candy, J. M. (1995) Copper binding to the N-terminal tandem repeat regions of mammalian and avian prion protein, *Biochem. Biophys. Res. Commun. 207*, 621−629.
40. Stöckel, J., Safar, J., Wallace, A. C., Cohen, F. E., and Prusiner, S. B. (1998) Prion protein selectively binds copper(II) ions, *Biochemistry 37*, 7185−7193.
41. Whittal, R. M., Ball, H. L., Cohen, F. E., Burlingame, A. L., Prusiner, S. B., and Baldwin, M. A. (2000) Copper binding to octarepeat peptides of the prion protein monitored by mass spectrometry, *Protein Sci. 9*, 332−343.
42. Aronoff-Spencer, E., Burns, C. S., Avdievich, N. I., Gerfen, G. J., Peisach, J., Antholine, W. E., Ball, H. L., Cohen, F. E., Prusiner, S. B., and Millhauser, G. L. (2000) Identification of the Cu^{2+} binding sites in the N-terminal domain of the prion protein by EPR and CD spectroscopy, *Biochemistry 39*, 13760−13771.
43. Viles, J. H., Cohen, F. E., Prusiner, S. B., Goodin, D. B., Wright, P. E., and Dyson, H. J. (1999) Copper binding to the prion protein: structural implications of four identical cooperative binding sites, *Proc. Natl. Acad. Sci. U.S.A. 96*, 2042−2047.
44. Garnett, A. P., and Viles, J. H. (2003) Copper binding to the octarepeats of the prion protein, *J. Biol. Chem. 278*, 6795−6802.
45. Jones, C. E., Abdelraheim, S. R., Brown, D. R., and Viles, J. H. (2004) Preferential Cu^{2+} coordination by His96 and His111 induces b-sheet formation in the unstructured amyloidogenic region of the prion protein, *J. Biol. Chem. 279*, 32018−32027.
46. Burns, C. S., Aronoff-Spencer, E., Legname, G., Prusiner, S. B., Antholine, W. E., Gerfen, G. J., Peisach, J., and Millhauser, G. L. (2003) Copper coordination in the full-length, recombinant prion protein, *Biochemistry 42*, 6794−6803.
47. Jackson, G. S., Murray, I., Hosszu, L., Gibbs, N., Waltho, J. P., Clarke, A. R., and Collinge, J. (2001) Location and properties of metal-binding sites on the human prion protein, *Proc. Natl. Acad. Sci. U.S.A. 98*, 8531−8535.
48. Cohlberg, J. A., Li, J., Uversky, V. N., and Fink, A. L. (2002) Heparin and other glycosaminoglycans stimulate the formation of amyloid fibrils from a-synuclein in vitro, *Biochemistry 41*, 1502−1511.
49. Brown, D. R., Hafiz, F., Glasssmith, L. L., Wong, B. S., Jones, I. M., Clive, C., and Haswell, S. J. (2000) Consequences of manganese replacement of copper for prion protein function and proteinase resistance, *EMBO J. 19*, 1180−1186.
50. Qin, K., Yang, Y., Mastrangelo, P., and Westaway, D. (2002) Mapping Cu(II) binding sites in prion proteins by diethyl pyrocarbonate modification and matrix assisted laser desorption ionization-time of flight (MALDI-TOF) mass spectrometric footprinting, *J. Biol. Chem. 277*, 1981−1990.
51. Bocharova, O. V., Breydo, L., Parfenov, A. S., Salnikov, V. V., and Baskakov, I. V. (2005) In vitro conversion of full length mammalian prion protein produces amyloid form with physical property of PrPSc, *J. Mol. Biol. 346*, 645−659.
52. Flechsig, E., Shmerling, D., Hegyi, I., Raeber, A. J., Fischer, M., Cozzio, A., von Mering, C., Aguzzi, A., and Weissmann, C. (2000) Prion protein devoid of the octapeptide repeat region restores susceptibility to scrapie in PrP knockout mice, *Neuron 27*, 399−408.
53. Zahn, R. (2003) The octapeptide repeats in mammalian prion protein constitue a pH-dependent folding and aggregqtion site, *J. Mol. Biol. 334*, 477−488.
54. Gonzalez-Iglesias, R., Elvira, G., Rodriguez-Navarro, J. A., Velez, M., Calero, M., Pajares, M. A., and Gasset, M. (2004) Cu2+ binding triggers aBoPrP assembly into insoluble laminar polymers, *FEBS Lett. 556*, 161−166.
55. Nishina, K., Jenks, S., and Supattapone, S. (2004) Ionic strength and transition metals control PrPSc protease resistance and conversion-inducing activity, *J. Biol. Chem. 279*, 40788−40794.
56. Chiesa, R., Piccardo, P., Quaglio, E., Drisaldi, B., Si−Hoe, S. L., Takao, M., Ghetti, B., and Harris, D. A. (2003) Molecular distinction between pathogenic and infectious properties of the prion protein, *J. Virol. 77*, 7622.
57. Wadsworth, J. D. F., Hill, A. F., Joiner, S., Jackson, G. S., Clarke, A. R., and Collinge, J. (1999) Strain-specific prion-protein conformation determined by metal ions, *Nat. Cell Biol. 1*, 55−59.
58. Notari, S., Capellari, S., Giese, A., Westner, I., Baruzzi, A., Ghetti, B., Gambetti, P., Kretzschmar, H. A., and Parchi, P. (2004) Effects of different experimental conditions on the PrPSc core generated by protease digestion, *J. Biol. Chem. 279*, 16797−16804.
59. Jimenez, J. L., Guijarro, J. I., Orlova, E., Zurdo, J., Dobson, C. M., Sunde, M., and Saibil, H. (1999) Cryo-electron microscopy structure of an SH3 amyloid fibril and model of the molecular packing, *EMBO J. 18*, 815−821.
60. Jimenez, J. L., Nettleton, E. J., Bouchard, M., Robinson, C. V., Dobson, C. M., and Saibil, H. (2002) The protofilament structure of insulin amyloid fibrils, *Proc. Natl. Acad. Sci. U.S.A. 99*, 9196−9201.

61. Lashuel, H. A., LaBrenz, S. R., Woo, L., Serpell, L. C., and Kelly, J. W. (2000) Protofilaments, filaments, ribbons, and fibrils from peptidomimetic self-assembly: implications for amyloid fibril formation and materials science, *J. Am. Chem. Soc. 122*, 5262−5277.
62. Jansen, R., Dzwolak, W., and Winter, R. (2005) Amyloidogenic self-assembly of insulin aggregates probed by high-resolution atomic force microscopy, *Biophys. J. 88*, 1344−1353.
63. Khurana, R., and Fink, A. L. (2000) Do parallel *β*-helix proteins have a unique Fourier transform infrared spectrum?, *Biophys. J. 78*, 994−1000.
64. Rachidi, W., Mange, A., Senator, A., Guiraud, P., Riondel, J., Benboubetral, M., Favier, A., and Lehmann, S. (2003) Prion infection impairs copper binding of cultured cells, *J. Biol. Chem. 278*, 14595−14598.
65. Vassallo, N., and Herms, J. (2003) Cellular prion protein function in copper homeostasis and redox signaling at the synaps, *J. Neurochem. 86*, 544.
66. Giese, A., Levin, J., Bertsch, U., and Kretzchmar, H. A. (2004) Effect of metal ions on de novo aggregation of full-length prion protein, *Biochem. Biophys. Res. Commun. 320*, 1240−1246.
67. Levin, J., Bertsch, U., Kretzchmar, H. A., and Giese, A. (2005) Single particle analysis of manganese-induced prion protein aggregates, *Biochem. Biophys. Res. Commun. 329*, 1200−1207.
68. Cereghetti, G. M., Schweiger, A., Glockshuber, R., and Doorslaer, S. V. (2001) Electron paramagnetic resonance evidance for binding of Cu2+ to the C-terminal domain of the murine prion protein, *Biophys. J. 81*, 516−525.
69. Cereghetti, G. M., Schweiger, A., Glockshuber, R., and Doorslaer, S. V. (2003) Stability and Cu(II) binding of prion protein variants related to inherited human prion diseases, *Biophys. J. 84*, 1985−1997.
70. Hasnain, S. S., Murphy, L. M., Strange, R. W., Grossmann, J. G., Clarke, A. R., Jackson, G. S., and Collinge, J. (2001) XAFS study of the high-affinity copper-binding site of human PrP90−231 and its low-resolution structure in solution, *J. Mol. Biol. 311*, 467−473.
71. Burns, C. S., Aronoff-Spencer, E., Dunham, C. M., Lario, P., Avdievich, N. I., Antholine, W. E., Olmstead, M.M., Vrielink, A., Gerfen, G. J., Peisach, J., Scott, W. G., and Millhauser, G. L. (2002) Molecular features of the copper binding sites in the octarepeat domain of the prion protien, *Biochemistry 41*, 4001.
72. Morante, S., Gonzalez-Iglesias, R., Potrich, C., Meneghini, C., Meyer-Klaucke, W., Menestrina, G., and Gasset, M. (2004) Inter- and intra-octarepeat Cu(II) site geometries in the prion protein: implications in Cu(II) binding cooperativity and Cu(II)-mediated assemblies, *J. Biol. Chem. 279*, 11753−11759.
73. DeArmond, S. J., Ironside, J. W., Bouzamondo, E., Peretz, D., and Fraser, J. R. (2004) Neuropathology of prion diseases, in *Prion Biology and Diseases* (Prusiner, S.B., ed), pp 777−856, Cold Spring Harbor Laboratory Press, Cold Spring Harbor, NY.
74. DeArmond, S. J., McKinley, M. P., Barry, R. A., Braunfeld, M. B., McColloch, J. R., and Prusiner, S. B. (1985) Identification of prion amyloid filaments in scrapie-infected brain, *Cell 41*, 221−235.
75. Weissmann, C. (2004) The state of the prion, *Nat. Rev. Microbiol. 2*, 861−871.
76. Baskakov, I. V., and Bocharova, O. V. (2005) In Vitro conversion of mammalian prion protein into amyloid fibrils displays unusual features, *Biochemistry 44*, 2339−2348.

BI050251Q